Available online at www.sciencedirect.com

ScienceDirect

Procedia Structural Integrity 28 (2020) 850–863

Structural Integrity Procedia

www.elsevier.com/locate/procedia

1st Virtual European Conference on Fracture

Structural integrity of deepwater composite pipes under combined thermal and mechanical loading

James C. Hastie[a,b,*], Igor A. Guz[a,b], Maria Kashtalyan[a,b]

[a]*School of Engineering, University of Aberdeen, UK*
[b]*Centre for Micro- and Nanomechanics (CEMINACS), School of Engineering, University of Aberdeen, UK*

Abstract

Thermoplastic composite pipe (TCP) is an ideal candidate to replace traditional steel pipes in deepwater applications where high specific strengths and moduli and corrosion resistance are desirable. TCP consists of three layers: an inner thermoplastic liner; structural fibre-reinforced multi-ply laminate; and an outer thermoplastic liner. During deepwater operation the pipe is subjected to thermal gradient, arising from the mismatch between internal fluid and external ocean temperatures, in combination with mechanical loads. In the present work, a 3D finite element (FE) model is used to investigate structural integrity of TCP under combined pressures, tension and thermal gradient by considering yielding of isotropic liners and failure of the laminate at ply-level according to existing stress-based criteria. Different orientations of reinforcing fibres are investigated.

Keywords: Thermoplastic composite pipe; offshore riser; thermomechanical analysis

1. Introduction

The advantages afforded by fibre-reinforced plastic (FRP) materials, including high specific strengths and moduli and excellent corrosion resistance, make them ideal candidates for subsea applications across multiple sectors, including underwater vehicles, marine construction and offshore oil and gas. Despite potential benefits, FRP usage in

* Corresponding author. *E-mail address:* r03jh15@abdn.ac.uk

10.1016/j.prostr.2020.11.053

offshore exploration and production (E&P) has historically been hindered by a reluctance to use "complex" materials where steels have generally proven to be fit-for-purpose. However, the spotlight is shifting to FRPs as E&P extends into deeper, harsher environments and the need arises for enabling and cost-effective solutions. In particular, spoolable FRP tubulars are being increasingly promoted for subsea and downhole applications (Menshykova and Guz, 2014; Cox et al., 2019).

Thermoplastic composite pipe (TCP) is an example of a spoolable product attracting growing interest for marine riser, hose and jumper applications. TCP consists of three layers, shown in Fig. 1: an inner thermoplastic liner; middle thermoplastic laminate, comprised of multiple fibre-reinforced plies stacked in particular orientations; and an outer thermoplastic liner. The laminate serves as the main structural layer with homogeneous liners providing protection and fluid-tightness. TCP is manufactured in continuous lengths using an automated process typified by leading manufacturers, during which the layers are melt-fused together to form a solid wall. The same thermoplastic is used throughout to achieve a fully consolidated bond. An industry standard has been developed in recent years to encourage uptake of TCP and standardise its design (DNV GL, 2018).

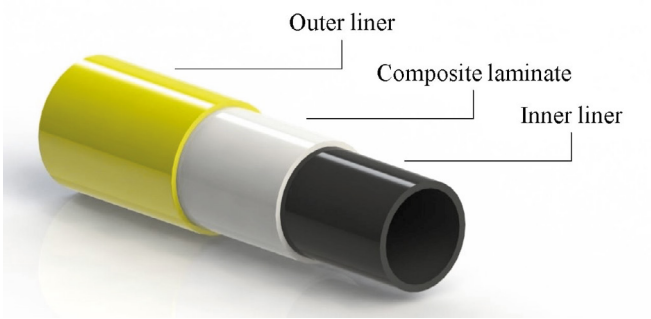

Fig. 1. TCP layers

A single-leg hybrid riser (SLHR) system, illustrated in Fig. 2, is an application in which TCP benefits can be exploited to great economic effect. Let us consider a section along the riser. During operation the section is subjected to internal and external surface pressures (P_0 and P_a) and axial tension (F_A) generated by a buoyancy module. Internal and external surface temperatures (T_0 and T_a) are generated from hot pipe contents and cool surrounding seawater.

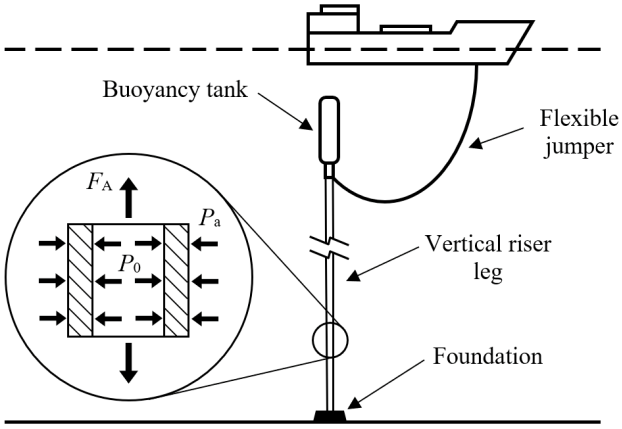

Fig. 2. SLHR system

The behaviour of composite pipes under mechanical loads including axisymmetric pressures and axial tension has been studied for many years. Early work by Rosenow (1984) showed that stress-strain response of FRP pipes under biaxial and hoop pressure loading can be predicted using lamination theory up to a point of nonlinearity. A fibre angle

of 54.75° from the longitudinal axis (typically rounded to 55°) results in a hoop-to-axial stress ratio of 2:1 for biaxial loading. Xia et al. (2001b) derived an exact solution for multi-layered FRP pipes under internal pressure based on 3D anisotropic elasticity. The hoop-to-axial stress ratio varies through plies of different angles. Yousefpour and Nejhad (2004) presented a design methodology for subsea laminated pressure vessels under external pressure based on nonlinear finite element (FE) modelling. Guz et al. (2017) reviewed applications of fibre-reinforced pipes in the oil and gas industry and presented an analytical stress solution for FRP pipes under external pressure. The approach can be developed for pipes that incorporate metallic layers for collapse resistance. The mechanical behaviour of a filament-wound composite tube with vulcanized rubber liners under uniaxial tension was investigated using FE modelling by Szabó et al. (2017). Xu et al. (2019) studied glass-reinforced thermoplastic pipe subjected to tension by experiments, FE modelling and analytical modelling accounting for material nonlinearity. The response of FRP pipes under tension combined with internal (Qiao et al., 2018) and external (Bai et al., 2014) pressures has also been studied analytically and numerically for offshore applications.

Literature relating to thermomechanical loading of composite pipes is less widely available. Relevant studies have largely been limited to analytical or semi-analytical modelling of pipes consisting of isotropic layers (Zhang et al., 2012), fibre-reinforced plies (Bakaiyan et al., 2009) or a 'sandwich' combination of the two (Xia et al., 2001a) under thermal load combined with pressure only. Numerical models developed using dedicated FE software would allow a wide array of combined mechanical and thermal loads to be investigated. Furthermore, defects such as delamination can be introduced and studied whilst this may prove analytically complex.

A 3D FE model capable of analysing stresses in a section of carbon fibre-reinforced plyetheretherketone (PEEK) TCP under combined thermal and mechanical loads illustrative of an SLHR application was recently developed by Hastie et al. (2019a). In this paper, the model is used to study structural integrity of TCP under different load combinations. Failure responses are compared based on a selection of lamina failure criteria for TCP with various fibre-reinforced ply orientations.

2. Numerical study

The FE model developed by Hastie et al. (2019a) is used to analyse stresses in TCP under combined surface pressures, axial tension and thermal gradient. Validation against an analytical solution for mechanical loading was previously shown (Hastie et al., 2019a). The model is described in the following section. In addition, a convergence exercise performed to inform creation of an appropriate mesh is presented here, as well as a validation of the use of 3D thermal elements for thermomechanical analysis of fibre-reinforced layers. Computed stresses are used to evaluate failure coefficient according to existing criteria summarised in Section 2.4.

2.1. Finite element model

A 24mm long section of TCP was modelled in Abaqus/CAE 2019. Section dimensions are given in Table 1. The laminate is comprised of eight plies of equal thickness. Assuming perfect bonding, a single 3D part is partitioned into layers with discrete material orientations assigned to FRP plies. Temperature-dependent material properties compiled from literature and listed by Hastie et al. (2019a) were used to define AS4/APC-2 carbon/PEEK laminate and neat APC-2 PEEK liners. The model is meshed using quadratic reduced integration thermal elements C3D20RT available in Abaqus. Combined mechanical and thermal loads are applied simultaneously in a coupled temperature-displacement step. Pressures P_0 and P_a are applied directly on internal and external surfaces. Axial tension F_A is applied on a reference point located at the centre of one pipe end, with the end face coupled to the reference point via a kinematic coupling, shown in Fig. 3, in all but the radial direction. The opposite end of the pipe is coupled to a fixed reference point. Temperature T_0 is applied as a fixed boundary condition on the internal surface. On the external surface, a surface film condition is applied to simulate free convection based on a transfer coefficient, h_a, and surrounding (ocean) temperature, T_∞.

Table 1. TCP section dimensions

Dimension	Value
Inner radius, r_0 (mm)	76
Inner liner thickness (mm)	8
Laminate thickness (mm)	8
Outer liner thickness (mm)	8
Outer radius, r_a (mm)	100

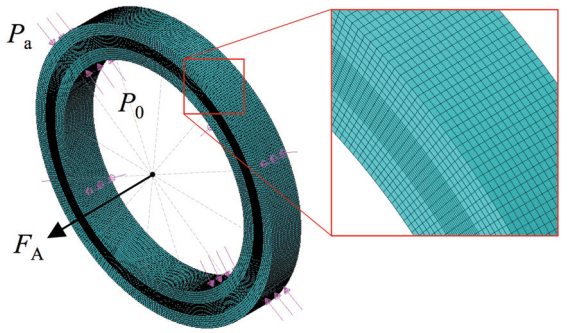

Fig. 3. TCP model and mechanical loads

2.2. Mesh convergence

A convergence exercise was undertaken to establish a suitable mesh. Refining element density in three directions concurrently is straightforward for a thick-walled single-layer pipe. However, efficient meshing of TCP is challenging due to FRP plies being much thinner than the liners. It is impractical to add elements through individual plies for every mesh in a refinement series. A methodical approach was adopted whereby meshes were created for the TCP outlined in Section 2.1 with $[\pm 55]_4$ laminate (plies arranged at alternating +/-55° from longitudinal pipe axis) based on one, two and three through-ply elements. Density was increased systematically in circumferential and axial directions, and in the radial direction through the liners only.

Simulations were run for the following load case: P_0=60MPa, P_a=30MPa, F_A=50kN, T_0=130°C, T_∞=4°C, h_a=50Wm^{-2}°C^{-1}. An initial temperature of T_{ref}=23°C is assumed. Fig. 4 and Fig 5 show liner von Mises and laminate principal stresses vs. mesh density. Adding through-ply elements does not significantly impact convergence within the liners. In the laminate, there is a noticeable difference between one and two through-ply elements but the effect of adding a third is small. The 'fine mesh' with two elements through each ply was deemed suitable. Relative to the densest mesh, the largest differences in liner and laminate stresses are 0.086% and 0.014% (σ_2) respectively. The mesh, visible in Fig. 3, comprises 28 through-wall elements (six through each liner and two through each FRP ply), 412 around the circumference and 18 along the length. A total of 207,648 elements and 888,272 nodes are used.

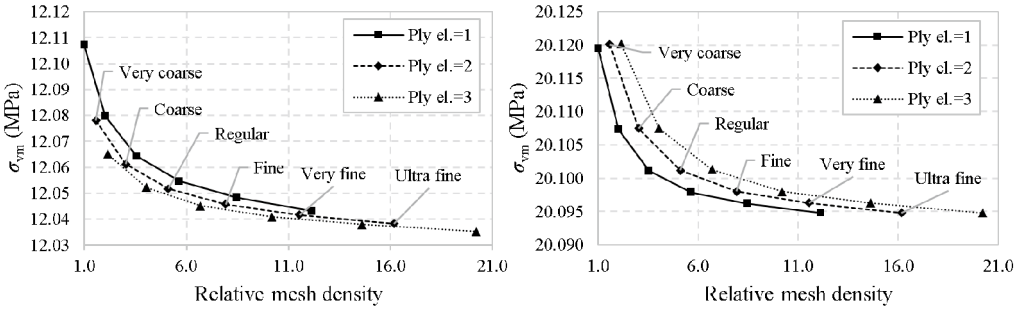

Fig. 4. Maximum von Mises stress in inner (left) and outer (right) liners: increasing mesh density for one, two and three through-ply elements

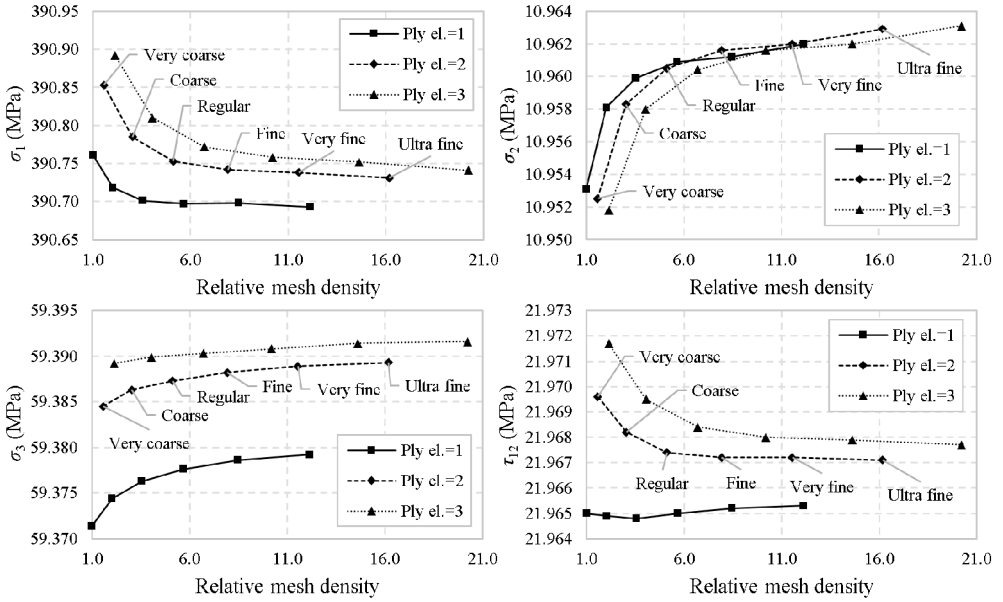

Fig. 5. Maximum stress magnitudes in laminate: increasing mesh density for one, two and three through-ply elements

2.3. Validation of thermal elements

To validate the use of C3D20RT elements in a coupled-temperature displacement step for analysing stress-state in composite pipe under thermomechanical load an FE model of the carbon/epoxy pipe studied by Bakaiyan et al. (2009) was created. The pipe has inner and outer radii r_0=50mm and r_a=51.2mm, is comprised of four unidirectional plies of equal thickness and has initial temperature T_{ref}=25°C. Applied pressure and surface temperatures are P_0=10MPa, T_0=147.3°C and T_a=140.4°C. A 20mm long 3D model was developed following the outline in Section 2.1. A comparison between cylindrical stresses presented by Bakaiyan et al. (2009) for $[\pm55]_2$ and $[(\pm35)/(90)_2]$ laminates and those obtained using the FE model is shown in Fig. 6. Close agreement verifies the suitability of C3D20RT elements for analysis of composite pipe under combined thermal and mechanical loading.

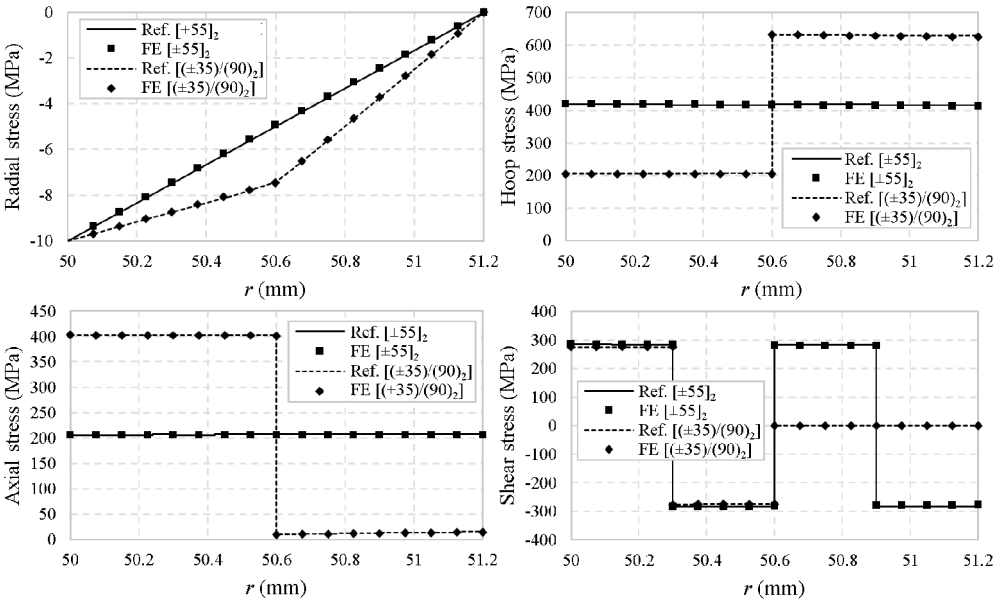

Fig. 6. Comparison of cylindrical stresses: FE validation model and reference study (Bakaiyan et al., 2009)

2.4. Failure criteria

In this study, TCP through-thickness failure coefficient is evaluated according to von Mises criterion for isotropic liners and Maximum Stress (herein "Max Stress"), Tsai-Hill and Hashin criteria for orthotropic laminate plies using stresses obtained by FE simulation.

The von Mises failure coefficient for isotropic liners is written as

$$f^{\mathrm{VM}} = \sqrt{\frac{(\sigma_1-\sigma_2)^2+(\sigma_2-\sigma_3)^2+(\sigma_3-\sigma_1)^2}{2}}\frac{1}{\sigma_y}, \tag{1}$$

where σ_y is the isotropic yield strength (failure occurs when f^{VM}=1).

Stresses in principal material coordinates are used to evaluate orthotropic ply failure. These are transformed from pipe cylindrical coordinates as follows:

$$\begin{Bmatrix}\sigma_1\\ \sigma_2\\ \sigma_3\\ \tau_{23}\\ \tau_{13}\\ \tau_{12}\end{Bmatrix} = \begin{bmatrix} m^2 & n^2 & 0 & 0 & 0 & 2mn \\ n^2 & m^2 & 0 & 0 & 0 & -2mn \\ 0 & 0 & 1 & 0 & 0 & 0 \\ 0 & 0 & 0 & m & -n & 0 \\ 0 & 0 & 0 & n & m & 0 \\ -mn & mn & 0 & 0 & 0 & m^2-n^2 \end{bmatrix} \begin{Bmatrix}\sigma_z\\ \sigma_\theta\\ \sigma_r\\ \tau_{\theta r}\\ \tau_{zr}\\ \tau_{z\theta}\end{Bmatrix}, \tag{2}$$

where m=cosφ and n=sinφ; φ is the fibre angle with respect to the pipe axial direction.

The Max Stress theory for an orthotropic ply assumes failure occurs simply when any stress component exceeds the corresponding allowable. The coefficient is

$$f^{\mathrm{MS}} = \max\left\{\frac{\sigma_1}{X_{\mathrm{T}}} or \frac{|\sigma_1|}{X_{\mathrm{C}}}, \frac{\sigma_2}{Y_{\mathrm{T}}} or \frac{|\sigma_2|}{Y_{\mathrm{C}}}, \frac{\sigma_3}{Z_{\mathrm{T}}} or \frac{|\sigma_3|}{Z_{\mathrm{C}}}, \frac{|\tau_{23}|}{Q}, \frac{|\tau_{13}|}{R}, \frac{|\tau_{12}|}{S}\right\}, \tag{3}$$

where X, Y and Z are tensile and compressive strengths (subscripts 'T' and 'C') along material directions 1, 2 and 3 respectively; Q, R, S are shear strengths in planes 23, 13, 12 respectively. Max Stress can be erroneous in instances of off-axis loading where interaction amongst stresses within the lamina becomes significant.

Azzi and Tsai (1965) proposed an interactive quadratic theory, commonly known as the Tsai-Hill criterion, based on Hill's modified von Mises criterion for homogenous anisotropic metals (Hill, 1948). The Tsai-Hill coefficient is

$$f^{\mathrm{TH}} = \frac{\sigma_1^2}{X_{\mathrm{T}}^2}+\frac{\sigma_2^2}{Y_{\mathrm{T}}^2}+\frac{\sigma_3^2}{Z_{\mathrm{T}}^2}-\sigma_1\sigma_2\left(\frac{1}{X_{\mathrm{T}}^2}+\frac{1}{Y_{\mathrm{T}}^2}-\frac{1}{Z_{\mathrm{T}}^2}\right)-\sigma_1\sigma_3\left(\frac{1}{X_{\mathrm{T}}^2}-\frac{1}{Y_{\mathrm{T}}^2}+\frac{1}{Z_{\mathrm{T}}^2}\right)-\sigma_2\sigma_3\left(-\frac{1}{X_{\mathrm{T}}^2}+\frac{1}{Y_{\mathrm{T}}^2}+\frac{1}{Z_{\mathrm{T}}^2}\right)+\frac{\tau_{23}^2}{Q^2}+\frac{\tau_{13}^2}{R^2}+\frac{\tau_{12}^2}{S^2}. \tag{4}$$

A limitation is the lack of distinction between tensile and compressive strengths and of any indication of failure mechanism. Furthermore, the adaptation of a ductile yielding theory for heterogeneous and brittle composites has drawn its criticism. Nonetheless the Tsai-Hill criterion is widely recognised. Other quadratic criteria, notably the most general polynomial proposed by Tsai and Wu (1971), can be regarded as purely curve-fitting and lacking of physical foundation.

Early work by Hashin and Rotem (1973) (subsequently expanded by Hashin (1980) and Puck and Schürmann (1998)) introduced physical-based criteria that describe heterogeneous failure mechanisms separately. Most generally, failure is described as fibre- or matrix-dominated and further categorised into failure by tension or compression.

Hashin's criterion (Hashin, 1980) distinguishes these four failure modes. Coefficients for the separate mechanisms are listed below.

Tensile fibre failure (when $\sigma_1 \geq 0$):

$$f^{\mathrm{H1}} = \max\left\{\left(\frac{\sigma_1}{X_{\mathrm{T}}}\right)^2 + \frac{(\tau_{12}^2+\tau_{13}^2)}{R^2}, \frac{\sigma_1}{X_{\mathrm{T}}}\right\}. \tag{5a}$$

Compressive fibre failure ($\sigma_1 < 0$):

$$f^{\mathrm{H2}} = \frac{|\sigma_1|}{X_{\mathrm{C}}}. \tag{5b}$$

Tensile matrix failure ($(\sigma_2+\sigma_3) > 0$):

$$f^{\mathrm{H3}} = \frac{(\sigma_2+\sigma_3)^2}{Y_{\mathrm{T}}^2} + \frac{(\tau_{23}^2-\sigma_2\sigma_3)}{Q^2} + \frac{(\tau_{12}^2+\tau_{13}^2)}{R^2}. \tag{5c}$$

Compressive matrix failure ($(\sigma_2+\sigma_3) < 0$):

$$f^{\mathrm{H4}} = \left(\left(\frac{Y_{\mathrm{C}}}{2Q}\right)^2 - 1\right)\frac{(\sigma_2+\sigma_3)}{Y_C} + \frac{(\sigma_2+\sigma_3)^2}{4Q^2} + \frac{(\tau_{23}^2-\sigma_2\sigma_3)}{Q^2} + \frac{(\tau_{12}^2+\tau_{13}^2)}{R^2}. \tag{5d}$$

3. Results and discussion

Failure predictions are compared for the TCP described in Section 2.1 with different FRP laminate stacking orientations operating under combined thermal and mechanical loads. The laminate configurations, designated 'A', 'B' and 'C', are outlined in Table 2. Internal-to-external pressure ratios of 1.5 and 2 are investigated for external pressure P_a=20MPa, corresponding to roughly 2,000m ocean depth. Internal temperatures of T_0=30 and 130°C and axial tensions of F_A=50 and 500kN are studied. An initial temperature of T_{ref}=23°C is assumed. The surrounding ocean temperature is T_∞=4°C with a heat transfer coefficient at the outer surface of h_a=50Wm^{-2}°C^{-1}.

Table 2. Laminate configurations

TCP	Laminate ply arrangement
A	$[\pm 55]_4$
B	$[\pm 42.5]_4$
C	$[(\pm 55)_2/(\pm 30)_2]$

3.1. Through-thickness temperature distribution

Through-thickness temperature distributions for T_0=30 and 130°C cases are shown in Fig. 7 (the configurations differ in fibre angle φ rotated about the radial direction; radial temperature distributions are identical for TCP A, B and C). Temperature at the outer surface exposed to free convection does not rise significantly with increasing T_0. The

drop in temperature is steeper through the liners (r=76 to 84mm, 92 to 100mm) than the laminate (r=84 to 92mm) due to lower through-liner conductivity and thus greater insulating characteristics.

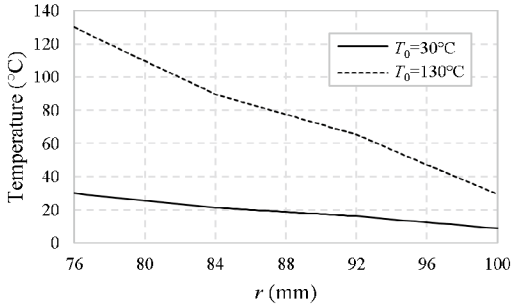

Fig. 7. Through-thickness temperature distribution

3.2. 30MPa internal pressure

Failure coefficients based on von Mises and Max Stress criteria through liners and laminate respectively are shown in Fig. 8 for P_0=30MPa (internal-to-external pressure ratio of 1.5). With increasing T_0 the liner coefficient rises considerably at the inner radius where temperature change is greatest as per Fig. 7. Distributions for all configurations are very similar under 50kN tension at both T_0=30 and 130°C. Coefficients through all layers of TCP A increase at 500kN, whereas the responses of B and C, which utilise lower fibre angles that provide greater axial reinforcement, do not change appreciably with tension. The von Mises/Max Stress distributions for TCP B and C laminates with plies orientated at ±42.5° or a combination of ±55 and ±30° respectively are close to identical.

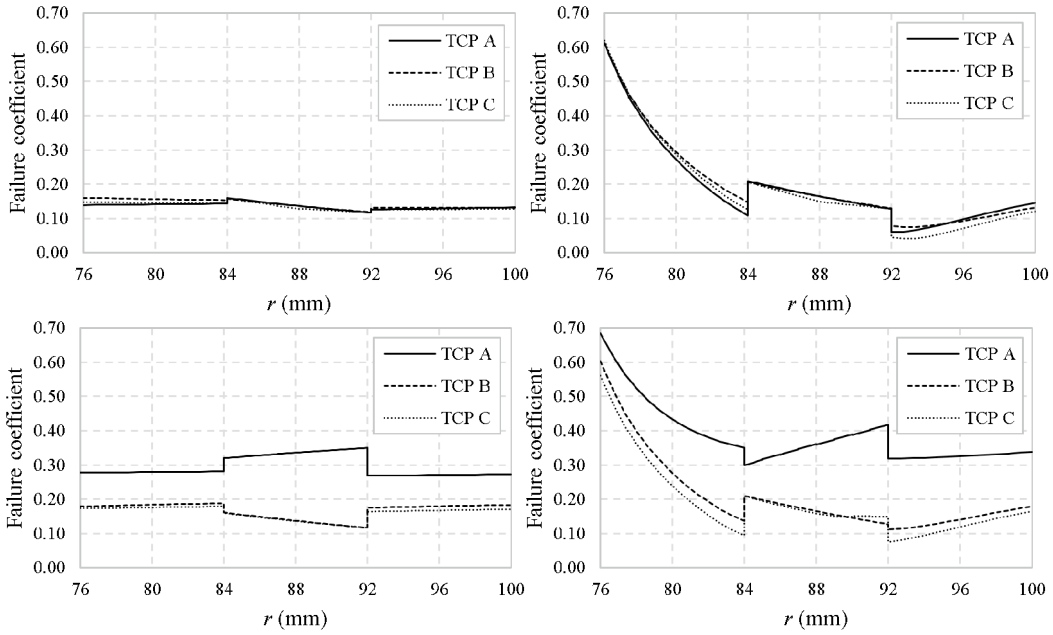

Fig. 8. Through-thickness failure coefficient based on von Mises criterion through liners and Max Stress criterion through laminate: P_0/P_a=30/20MPa; T_0=30 (left), 130°C (right); F_A=50 (top), 500kN (bottom)

Through-laminate Tsai-Hill coefficients are shown in Fig. 9 for internal-to-external pressure ratio of 1.5. Again, distributions for all configurations are not significantly dissimilar under 50kN tension. TCP A exhibits large Tsai-Hill coefficient under 500kN, particularly at T_0=130°C. Significantly higher Tsai-Hill with respect to Max Stress coefficient for TCP A highlights the importance of accounting for stress interaction under the combined loads.

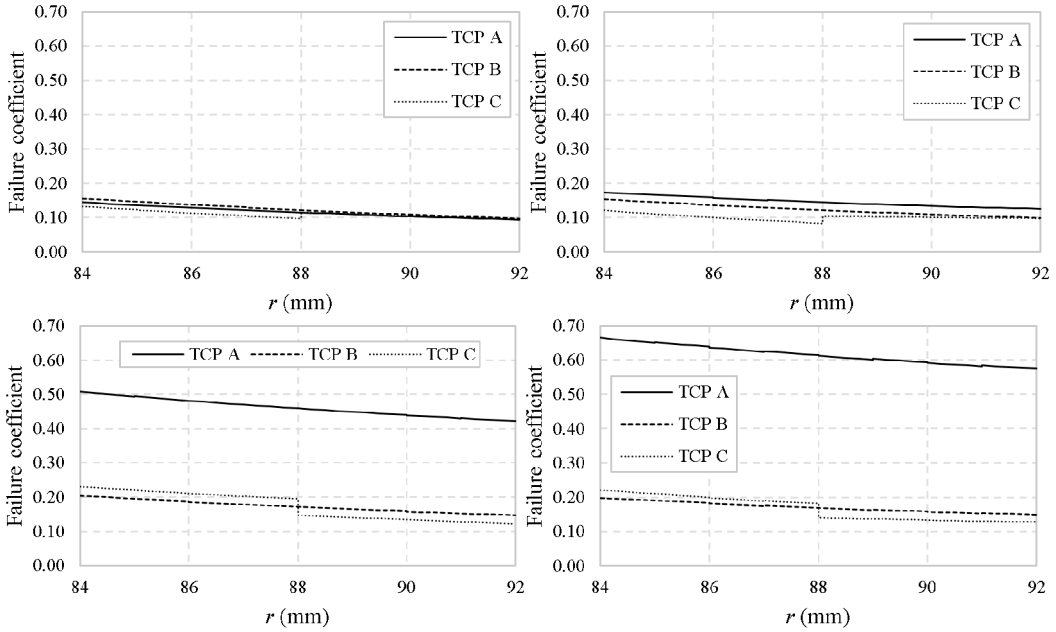

Fig. 9. Through-laminate Tsai-Hill coefficient: P_0/P_a=30/20MPa; T_0=30 (left), 130°C (right); F_A=50 (top), 500kN (bottom)

Distributions of Hashin coefficient through the laminates are shown in Fig. 10 for pressure ratio of 1.5. Hashin failure predictions are generally lower than those of Max Stress and Tsai-Hill criteria in this study. TCP A again exhibits sub-optimal failure coefficient for F_A=500kN. The coefficient is highest through the ±55° region (innermost plies) of TCP C at 50kN and conversely through the ±30° region (outermost plies) at 500kN. The opposite is true for Tsai-Hill distributions shown in Fig. 9, albeit the Tsai-Hill coefficient varies less through the different angle regions. TCP B is superior under all four temperature and tension combinations in terms of lower maximum Hashin coefficient overall.

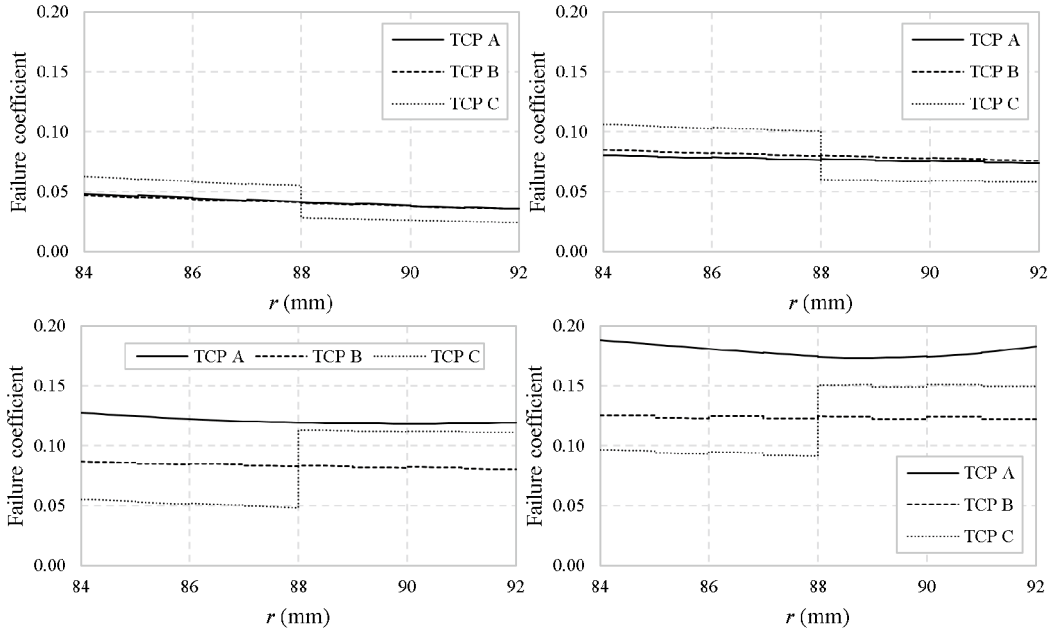

Fig. 10. Through-laminate Hashin coefficient: P_0/P_a=30/20MPa; T_0=30 (left), 130°C (right); F_A=50 (top), 500kN (bottom)

A summary of laminate failure coefficients is presented in Table 3, which includes Max Stress and Hashin failure modes. The latest industry standard for TCP dictates that the Max Stress criterion be satisfied with other criteria permissible provided they are comparatively "equal or conservative" (DNV GL, 2018). Tsai-Hill coefficients are lower than Max Stress for all 50kN cases and higher (more conservative) for 500kN cases with the exception of TCP C at T_0=130°C. Differences between Max Stress and interactive failure criteria are common in cases of off-axis loading where stress interaction is significant. The disparity is most notable for TCP A under 500kN where Max Stress coefficient is governed by transverse tension. The dominant mode for all other load cases is out-of-plane (radial) compression. Hashin coefficients are noticeably lower than Max Stress and Tsai-Hill coefficients as previously mentioned. The critical Hashin mode is fibre tension for the majority of cases with matrix compression only critical in TCP A under 500kN.

Table 3. Laminate failure coefficients: P_0/P_a=30/20MPa

F_A (kN)	T_0 (°C)	TCP	Max Stress		Tsai-Hill	Hashin	
			Coefficient	Mode	Coefficient	Coefficient	Mode
50	30	A	0.160	Out-of-plane compression	0.144	0.048	Fibre in tension
		B	0.158	Out-of-plane compression	0.156	0.047	Fibre in tension
		C	0.159*	Out-of-plane compression	0.133*	0.063*	Fibre in tension
	130	A	0.209	Out-of-plane compression	0.173	0.080	Fibre in tension
		B	0.206	Out-of-plane compression	0.153	0.085	Fibre in tension
		C	0.207*	Out-of-plane compression	0.121*	0.106*	Fibre in tension
500	30	A	0.350	Transverse tension	0.507	0.127	Matrix in compression
		B	0.161	Out-of-plane compression	0.204	0.087	Fibre in tension
		C	0.160*	Out-of-plane compression	0.231*	0.113**	Fibre in tension
	130	A	0.418	Transverse tension	0.665	0.188	Matrix in compression
		B	0.210	Out-of-plane compression	0.198	0.125	Fibre in tension
		C	0.208*	Out-of-plane compression	0.221*	0.151**	Fibre in tension

*±55° ply; **±30° ply

3.3. 40MPa internal pressure

Here, we consider P_0=40MPa (internal-to-external pressure ratio of 2). Failure distributions based on von Mises and Max Stress criteria are shown in Fig. 11. Laminate Tsai-Hill and Hashin coefficients are shown in Fig. 12 and Fig. 13. As witnessed for both tensions at lower P_0, the inner liner failure coefficient rises drastically with T_0 at 50kN. Increasing T_0 has less effect on the TCP under 500kN. In practical terms, a wider range of operating temperatures may be available to the designer for large pressure differential and tension. Circumferential reinforcement is beneficial under large pressure and TCP A exhibits relatively low liner and laminate coefficients for 50kN cases. As with P_0=30MPa, Max Stress and Tsai-Hill coefficients are highest for TCP A at 500kN. However, the overall response of TCP A does not change significantly when increasing P_0 from 30 to 40MPa. On the other hand, TCP B and C exhibit higher Max Stress and Tsai-Hill coefficients under larger P_0. In other words, a balanced ±55° laminate outperforms the lower angle configurations under low pressure differential and tension and improvements in Max Stress and Tsai-Hill coefficients afforded by lower angles under high tension are less pronounced. The Hashin coefficient is in fact slightly lower for TCP A in comparison with B and C under high tension. One can deduce that TCP B and C become less effective under higher pressures.

Of the configurations studied, TCP C exhibits the optimal Tsai-Hill coefficient for P_0/P_a=40/20MPa, F_A=500kN. At 50kN, the Tsai-Hill response of TCP C is inferior to A ($[\pm 55]_4$) but superior to B ($[\pm 42.5]_4$). This demonstrates that combining plies orientated at ±55° with lower angles also offers an improvement over balanced low angle laminates

under high pressure and low tension. Moreover, TCP C is comparable with A in terms of laminate Max Stress coefficients at 50kN. The Hashin coefficient is slightly larger through the ±55° region of TCP C in relation to the other configurations. From a design point-of-view the Hashin coefficient would not be considered critical if considering the different failure criteria equally and concurrently, given that it is markedly lower than Tsai-Hill. It was previously shown that orientating the innermost plies at ±55° and outermost at ±30° is superior to the reverse order in terms of Tsai-Hill coefficient under combined pressures, tension and thermal gradient (Hastie et al., 2019b).

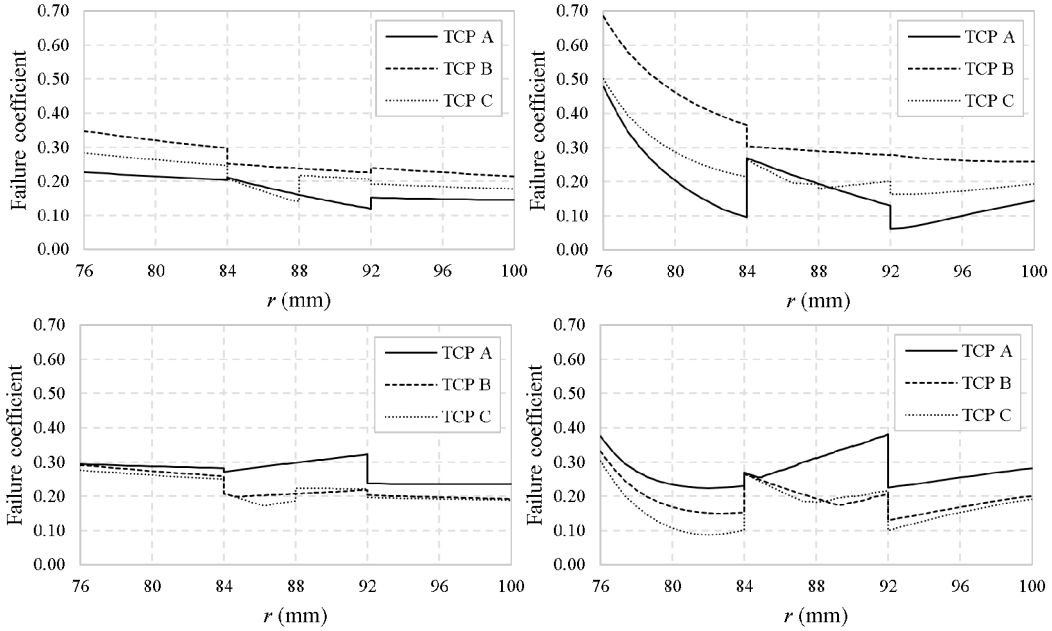

Fig. 11. Through-thickness failure coefficient based on von Mises criterion through liners and Max Stress criterion through laminate: P_0/P_a=40/20MPa; T_0=30 (left), 130°C (right); F_A=50 (top), 500kN (bottom)

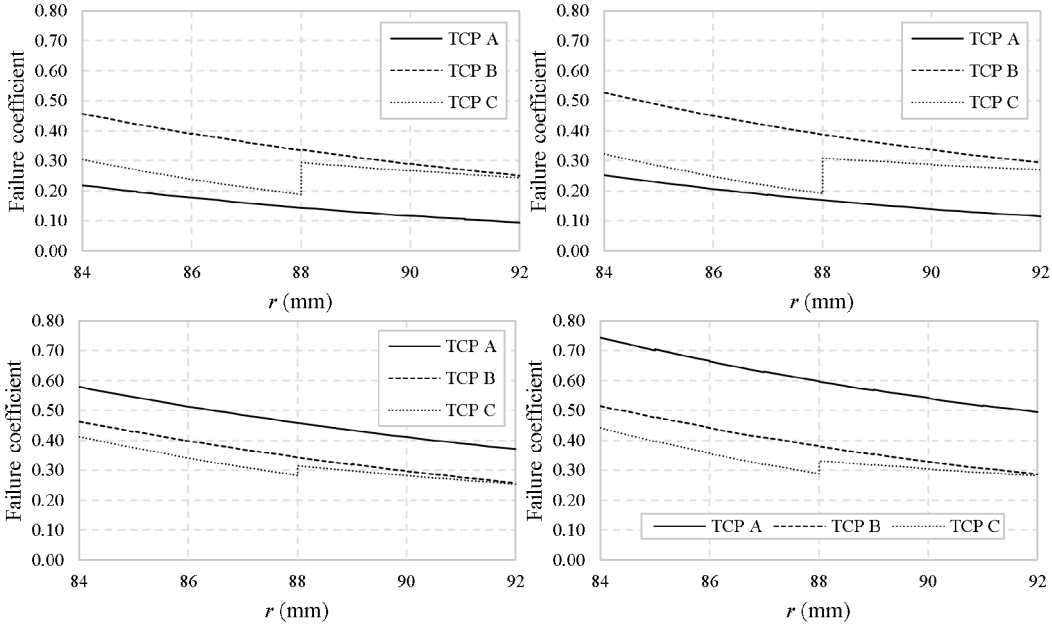

Fig. 12. Through-laminate Tsai-Hill coefficient: P_0/P_a=40/20MPa; T_0=30 (left), 130°C (right); F_A=50 (top), 500kN (bottom)

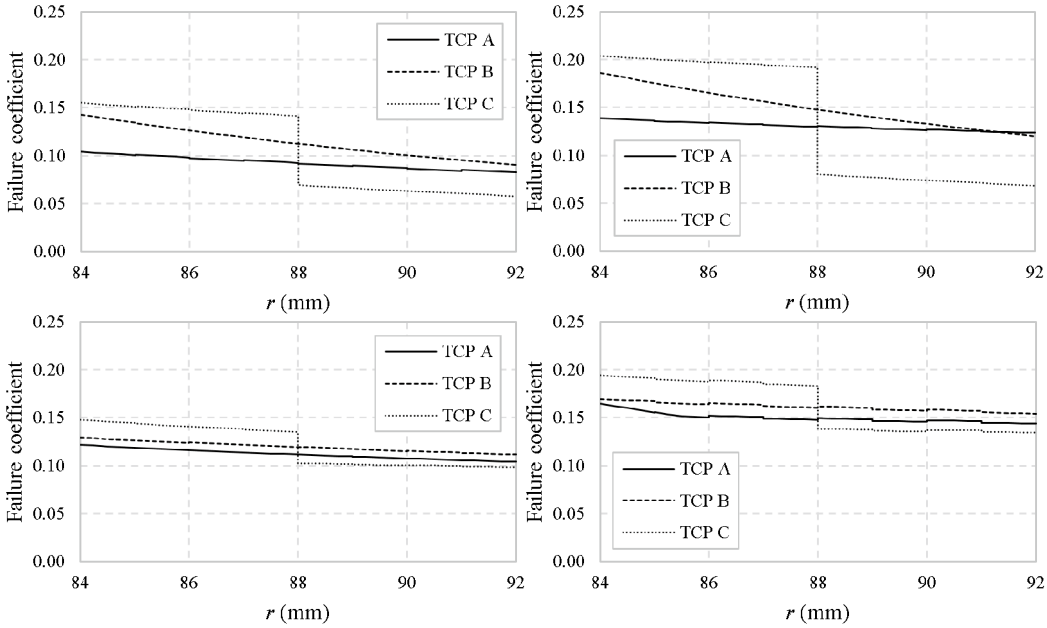

Fig. 13. Through-laminate Hashin coefficient: P_0/P_a=40/20MPa; T_0=30 (left), 130°C (right); F_A=50 (top), 500kN (bottom)

Failure coefficients and modes are summarised in Table 4 for internal-to-external pressure ratio of 2. The Tsai-Hill criterion is more conservative than Max Stress in all cases and particularly high in TCP A under 500kN, again emphasising the importance of stress interaction. We recall from Table 3 that Max Stress coefficients for all configurations under P_0/P_a=30/20MPa are governed by out-of-plane compression except for TCP A, governed by transverse tension for F_A=500kN. Dominant utilisation of in-plane shear and transverse tensile strengths is more prevalent for the case of P_0/P_a=40/20MPa. As before, Hashin coefficients are mostly governed by fibre tension and consistently less conservative than Max Stress. Therefore, use of Hashin criterion in practical design of TCP for the loads studied here would not satisfy current industry guidelines (DNV GL, 2018).

Table 4. Laminate failure coefficients: P_0/P_a=40/20MPa

F_A (kN)	T_0 (°C)	TCP	Max Stress		Tsai-Hill	Hashin	
			Coefficient	Mode	Coefficient	Coefficient	Mode
50	30	A	0.210	Out-of-plane compression	0.218	0.104	Fibre in tension
		B	0.252	In-plane shear	0.456	0.143	Matrix in compression
		C	0.218**	Transverse tension	0.304*	0.155*	Fibre in tension
	130	A	0.270	Out-of-plane compression	0.253	0.139	Fibre in tension
		B	0.303	In-plane shear	0.526	0.186	Matrix in compression
		C	0.265*	Out-of-plane compression	0.323*	0.204*	Fibre in tension
500	30	A	0.322	Transverse tension	0.578	0.122	Fibre in tension
		B	0.218	Transverse tension	0.462	0.129	Fibre in tension
		C	0.224**	Transverse tension	0.412*	0.148*	Fibre in tension
	130	A	0.380	Transverse tension	0.743	0.165	Matrix in compression
		B	0.264	Out-of-plane compression	0.515	0.169	Fibre in tension
		C	0.266*	Out-of-plane compression	0.442*	0.194*	Fibre in tension

*±55° ply; **±30° ply

4. Conclusions

In this work, a 3D FE model was used to analyse stress state in a section of TCP under combined thermal and mechanical loading illustrative of deepwater riser operation. Combinations of low and high axial tensions and thermal gradients for internal-to-external pressure ratios of 1.5 and 2 were simulated. Through-thickness failure coefficients were evaluated for different fibre-reinforced ply orientations using existing stress-based criteria. Temperature dependency of material properties was considered.

Increasing pipe internal temperature causes a rise in liner coefficient that is less severe under high internal-to-external pressure and tension. In practical terms a wider range of operating temperatures may be feasible in combination with large mechanical loads. Low fibre angle configurations are optimal for high tension combined with low pressure differential. However, the effectiveness of low angle plies diminishes at higher internal-to-external pressure. Combining plies orientated at ±55° with lower angle plies can offer a potentially attractive balance between circumferential and axial reinforcement.

The Tsai-Hill criterion was found to be more conservative than the Max Stress criterion for larger pressure ratio at both low and high tensions. Its selection for design for such loads would satisfy current industry guidelines. Conversely, the Hashin criterion consistently predicted lower failure coefficients and therefore would not satisfy current design rules. Extensive experimental work is needed to assess the accuracy of these and other proposed criteria for predicting laminate failure under combined thermal and mechanical loading. This can be undertaken with a view to refining industry guidelines and improving material utilisation, i.e. enabling design with less conservative safety factors. Nevertheless, the comparisons in this study provide useful insight into criteria selection for practical design in line with the latest guidelines.

References

Azzi, V.D., Tsai, S.W., 1965. Anisotropic strength of composites. Experimental Mechanics 5, 283–288.

Bai, Y., Xu, W., Cheng, P., Wang, N., Ruan, W., 2014. Behaviour of reinforced thermoplastic pipe (RTP) under combined external pressure and tension. Ships and Offshore Structures 9 (4), 464-474.

Bakaiyan, H., Hosseini, H., Ameri, E., 2009. Analysis of multi-layered filament-wound composite pipes under combined internal pressure and thermomechanical loading with thermal variations. Composite Structures 88 (4), 532-541.

Cox, K., Menshykova, M., Menshykov, O., Guz, I., 2019. Analysis of flexible composites for coiled tubing applications. Composite Structures 225, 111118.

DNV GL, 2018. Standard DNVGL-ST-F119 Thermoplastic Composite Pipes.

Guz, I.A., Menshykova, M., Paik, J.K., 2017. Thick-walled composite tubes for offshore applications: an example of stress and failure analysis for filament-wound multi-layered pipes. Ships and Offshore Structures 12 (3), 304-322.

Hashin, Z., 1980. Failure criteria for unidirectional fiber composites. Journal of Applied Mechanics 47 (2), 329-334.

Hashin, Z., Rotem, A., 1973. A fatigue failure criterion for fiber reinforced materials. Journal of Composite Materials 7 (4), 448-464.

Hastie, J.C., Guz, I.A., Kashtalyan, M., 2019a. Effects of thermal gradient on failure of a thermoplastic composite pipe (TCP) riser leg. International Journal of Pressure Vessels and Piping 172, 90-99.

Hastie, J.C., Kashtalyan, M., Guz, I.A., 2019b. Failure analysis of thermoplastic composite pipe (TCP) under combined pressure, tension and thermal gradient for an offshore riser application. International Journal of Pressure Vessels and Piping 178, 103998.

Hill, R., 1948. A theory of the yielding and plastic flow of anisotropic metals. Proceedings of the Royal Society of London. Series A, Mathematical and Physical Sciences 193 (1033), 281-297.

Menshykova, M., Guz, I.A., 2014. Stress analysis of layered thick-walled composite pipes subjected to bending loading. International Journal of Mechanical Sciences 88, pp.289-299.

Puck, A., Schürmann, H., 1998. Failure analysis of FRP laminates by means of physically based phenomenological models. Composites Science and Technology 58 (7), 1045-1067.

Qiao, H., Zhang, Y., Bai, Y., Cheng, P., Lu, Y., Han, P., Tang, G., 2018. Study on reinforced thermoplastic pipe under combined tension and internal pressure. Ships and Offshore Structures 13 (sup1), 86-97.

Rosenow, M.W.K., 1984. Wind angle effects in glass fibre-reinforced polyester filament wound pipes. Composites 15 (2), 144-152.

Szabó, G., Váradi, K., Felhős, D., 2017. Finite element model of a filament-wound composite tube subjected to uniaxial tension. Modern Mechanical Engineering 7 (4), 91-112.

Tsai, S.W., Wu, E.M., 1971. A General Theory of strength for anisotropic materials. Journal of Composite Materials 5 (1), 58-80.

Xia, M., Kemmochi, K., Takayanagi, H., 2001a. Analysis of filament-wound fiber-reinforced sandwich pipe under combined internal pressure and thermomechanical loading. Composite Structures 51 (3), 273-283.

Xia, M., Takayanagi, H., Kemmochi, K., 2001b. Analysis of multi-layered filament-wound composite pipes under internal pressure. Composite Structures 53 (4), 483-491.

Xu, Y., Bai, Y., Fang, P., Yuan, S., Liu, C., 2019. Structural analysis of fibreglass reinforced bonded flexible pipe subjected to tension. Ships and Offshore Structures 14 (7), 777-787.

Yousefpour, A., Nejhad, M.N.G., 2004. Design, analysis, manufacture, and test of APC-2/AS4 thermoplastic composite pressure vessels for deep water marine applications. Journal of Composite Materials 38 (19), 1701-1732.

Zhang, Q., Wang, Z.W., Tang, C.Y., Hu, D.P., Liu, P.Q., Xia, L.Z., 2012. Analytical solution of the thermo-mechanical stresses in a multilayered composite pressure vessel considering the influence of the closed ends. International Journal of Pressure Vessels and Piping 98, 102-110.